Geophysical Research Letters

RESEARCH LETTER
10.1029/2022GL099332

The Relationship Between Reflectivity and Rainfall Rate From Rain Size Distributions Observed in Hurricanes

Hua Leighton[1,2], Robert Black[2], Xuejin Zhang[2], and Frank D. Marks Jr.[2]

[1]Rosenstiel School of Marine and Atmospheric Science, University of Miami, Cooperative Institute for Marine & Atmospheric Studies, Miami, FL, USA, [2]NOAA/AOML/Hurricane Research Division, Miami, FL, USA

Key Points:

- The scatter in reflectivity (Z) -rainfall rate (R) distribution increases up to 48 dBZ or 25 mm hr^{-1}, after which it decreases rapidly
- There are significant uncertainties associated with using a power law Z-R relationship to estimate rainfall rate from radar reflectivity
- The result from a machine learning model shows that rainfall estimation is improved if drop size information and reflectivity are both used

Supporting Information:

Supporting Information may be found in the online version of this article.

Correspondence to:

H. Leighton,
chenhua@rsmas.miami.edu

Citation:

Leighton, H., Black, R., Zhang, X., & Marks, F. D. Jr. (2022). The relationship between reflectivity and rainfall rate from rain size distributions observed in hurricanes. *Geophysical Research Letters*, *49*, e2022GL099332. https://doi.org/10.1029/2022GL099332

Received 27 APR 2022
Accepted 21 OCT 2022

Author Contributions:

Conceptualization: Hua Leighton
Data curation: Robert Black
Formal analysis: Hua Leighton
Funding acquisition: Xuejin Zhang
Investigation: Hua Leighton
Methodology: Hua Leighton
Software: Robert Black
Writing – original draft: Hua Leighton
Writing – review & editing: Hua Leighton, Robert Black, Xuejin Zhang, Frank D. Marks

Abstract Raindrop size distributions collected by the DROPLET MEASUREMENT TECHNOLogies Precipitation imaging probe from 17 flights through 6 hurricanes during National Oceanic and Atmospheric Administration's hurricane field program in 2020 are used to study reflectivity (Z) and rainfall rate (RR) (R) relationship (i.e., Z-R relationship). The results show that the Z-R distribution is highly scattered and the scatter increases with RR and reflectivity up to 48 dBZ or 25 mm hr^{-1}, after which it decreases rapidly. The range of the estimated RR from a power-law Z-R relationship can be as large as 50 mm hr^{-1} at reflectivity of 40 dBZ. The result from random forest regression model demonstrates that including the information of mass-weighted-diameter (D_m) along with radar reflectivity improves the estimated RR significantly.

Plain Language Summary One of the main applications of radar measurements is to estimate rainfall rate (RR) based on its power-law relationships with radar reflectivity. Different relationships have been obtained for different weather scenarios. Hurricanes, in comparison with other severe weather systems, have a much longer life cycle and travel across much greater zonal and meridional extent. Therefore, in order to accurately estimate the RR for a specific time at a specific location in a hurricane, the power-law relationship with constant coefficients needs to be improved. The uncertainties of the estimated RR using power-law relationship are related to the raindrop sizes. The usage of a machine learning model (random forest regression) demonstrates that the uncertainties in the estimated rainfall are reduced significantly when both radar reflectivity and the drop sizes are taken into account.

1. Introduction

Early studies (e.g., Atlas & Chmela, 1957; Marshall & Palmer, 1948) showed that there are statistical differences in the characteristics of the raindrop size distribution (RSD) between different systems. For example, RSDs in tropical convection are characterized by narrow spectra and small means in diameter yet RSDs in continental convection tend to have wider spectra and larger mean diameters. However, studies (Donnadieu, 1982; Ulbrich, 1983; Waldvogel, 1974) also pointed out that the differences in RSDs between different systems can be as large as those found from moment to moment within a given rainfall type. Hurricanes, in comparison with other severe weather systems, have a much longer life cycle and travel across much greater zonal and meridional extent. These characteristics imply that uncertainties and variabilities of RSDs are particularly high in hurricanes.

RSDs have received wide attention in meteorology for decades. One of the most important applications of RSDs is using Z-R relationship to estimate rainfall rate. Z and R are calculated as in Equations 1 and 2.

$$Z = \sum_i N(D_i) D_i^6 \tag{1}$$

$$R = \frac{1}{6\pi} \sum_i N(D_i) D_i^3 V_T(D_i) \tag{2}$$

D_i in Equations 1 and 2 represent the diameter in the designated size bin. $N(D_i)$ refers to the number of raindrops in the size bin. $V_T(D_i)$ in Equation 2 represents the terminal velocity as the function of raindrop size. A statistical Z-R relationship can thus be developed from the observed RSDs based on Equations 1 and 2. Battan (1973) has tabulated over 60 Z-R relationships based on measurements taken around the world. There are many more Z-R relationships documented in the literature since Battan (1973). However, only a few Z-R relations were developed from observations collected in hurricanes. Jorgensen and Willis (1982) (JW1982 hereafter) obtained

$Z = 300\ R^{1.35}$ using the Particle Measurement Systems 2D-P (precipitation) probe data collected from four flights into three hurricanes. Two other *Z-R* relationships, $Z = 287\ R^{1.27}$ and $Z = 301\ R^{1.38}$ for eyewall and rainbands respectively, were further obtained from two flights through Hurricane Frederic. Chang et al. (2009) presented $Z = 207\ R^{1.45}$ using RSDs collected by 2D video disdrometer and C-band polarimetric radar from 13 western Pacific typhoons that made landfall in Taiwan. Wen et al. (2018) found that $Z = 147\ R^{1.38}$ using RSDs collected by 2D video disdrometer from 7 typhoons that made landfall in China. These studies show that both the coefficient A and the exponent *b* in the *Z-R* relationship formulation vary significantly for tropical cyclone systems. In particular, Ulbrich and Lee (2002) studied rainfall characteristics associated with the remnants of Tropical Storm Helene using RSD data obtained from a standard RD69 Joss-Waldvogel (JW) raindrop disdrometer. They found that there were pronounced variations in the *Z-R* relationship from day-to-day and within a day that would limit the accuracy of the estimated rainfall from radar measurement. The pronounced differences in *Z-R* relations pose a great challenge for using a power-law *Z-R* relationship with a constant coefficient and exponent to estimate rainfall rate.

In this study, we use RSD data collected by the Droplet Measurement Technologies precipitation imaging probe (PIP) from 17 flights through 6 hurricanes during National Oceanic and Atmospheric Administration's hurricane field program in 2020 to study *Z-R* relationship in hurricanes. The remainder of the paper is organized as follows. In Section 2, the data processing and overall statistics of the data are provided; in Section 3, *Z-R* relationships from this study are presented; in Section 4, the comparison with early *Z-R* relationships in the literature are discussed; in Section 5, a machine learning model is employed to improve *Z-R* relationship. A conclusion is given in Section 6.

2. Data

The RSD observations used in this study are from 17 flights into 6 hurricanes in 2020: Four flights from Hanna, three flights from Isaias, two flights from Laura, three flights from Sally, one flight from Zeta, and foure flights from Delta. Observations taken outside the 500-km radius of the storm center are excluded from this study. Twenty samples with liquid water content (LWC) >12 g m^{-3} are also excluded. The number of total samples used in this study is 18,076.

Figure 1 presents the overall distribution of directly measured variables (e.g., wind speed, vertical wind, and altitude) and integral rain variables (e.g., LWC, reflectivity, rainfall rate, mass-weighted-diameter D_m, and total

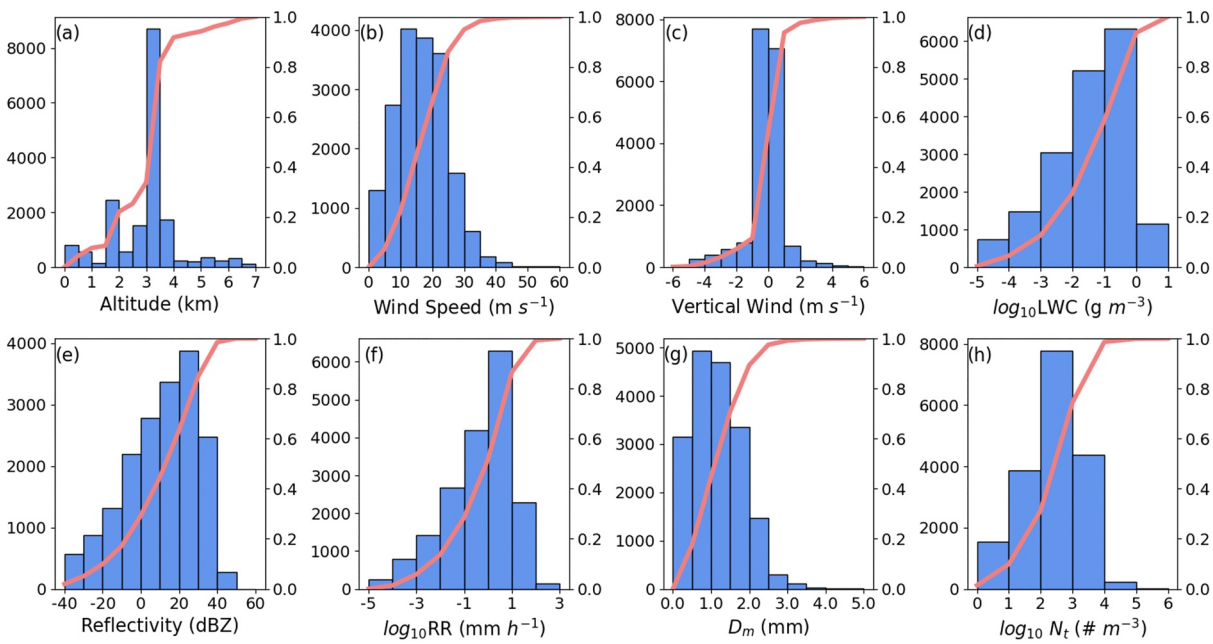

Figure 1. Histogram of (a) altitude, (b) wind speed, (c) vertical wind, (d) liquid water content in log scale, (e) reflectivity, (f) rainfall rate (RR) in log scale, (g) mass-weighted-diameter D_m, and (h) total number concentration N_t in log scale for the 18,076 samples in this study. The red curve in each plot denotes the corresponding cumulative distribution function.

number concentration N_t) calculated from the observed RSDs. The purpose of this figure is to provide references to what the distribution of RSDs and the integrated rain variables look like in the sample space. Even though the sample size is significantly larger than many studies that have focused on RSDs in hurricanes, it still might not be representative of all hurricane RSDs. The differences in the RSDs from one storm to another storm, from one flight to another flight, could exist.

As shown in Figure 1a, ~50% of observations are taken between 3 and 3.5-km altitude, where eyewall penetrations typically occur. About 85% of the observations occur at wind speeds less than 25 m s^{-1} and 82% percent of the data have vertical wind magnitudes less than 1 m s^{-1}. As pointed out in Black and Hallett (2012), strong-convection regions tend to be underrepresented in newer data (2005 and later) since flights specifically avoid penetrations of high-reflectivity areas. About 95% of samples have LWC less than 1 g m^{-3} 85% of samples have reflectivity less than 40 dBZ. About 87% of samples have rainfall rates less than 10 mm hr-1 Figures 1g and 1h show mass-weighted-diameter D_m, and total number concentration N_t. The D_m, which is calculated as the fourth-moment of RSD divided by the third-moment, has been widely used in RSD studies (e.g., Ulbrich, 1983) because of its reduced sensitivity to sampling limitations for small drop sizes, a problem for many instruments that measure drop size distributions (Steiner et al., 2004). Around 90% of samples have D_m less than 2 mm. Figure 1 shows that around 75% of samples have N_t less than 1,000 drops m^{-3} and around 99% less than 10,000 drops m^{-3}.

The procedure of data processing can be found in the Supporting Information S1.

3. *Z-R* Relationships in Hurricanes

Figure 2 shows the scatter plots of *Z-R* in log scale for four precipitation groups: stratiform precipitation at H (height) > 3-km altitude, stratiform precipitation at $H \leq 3$ km, convective precipitation at $H > 3$ km, and convective precipitation at $H \leq 3$ km. The threshold values we adopt to stratify stratiform precipitation and convective

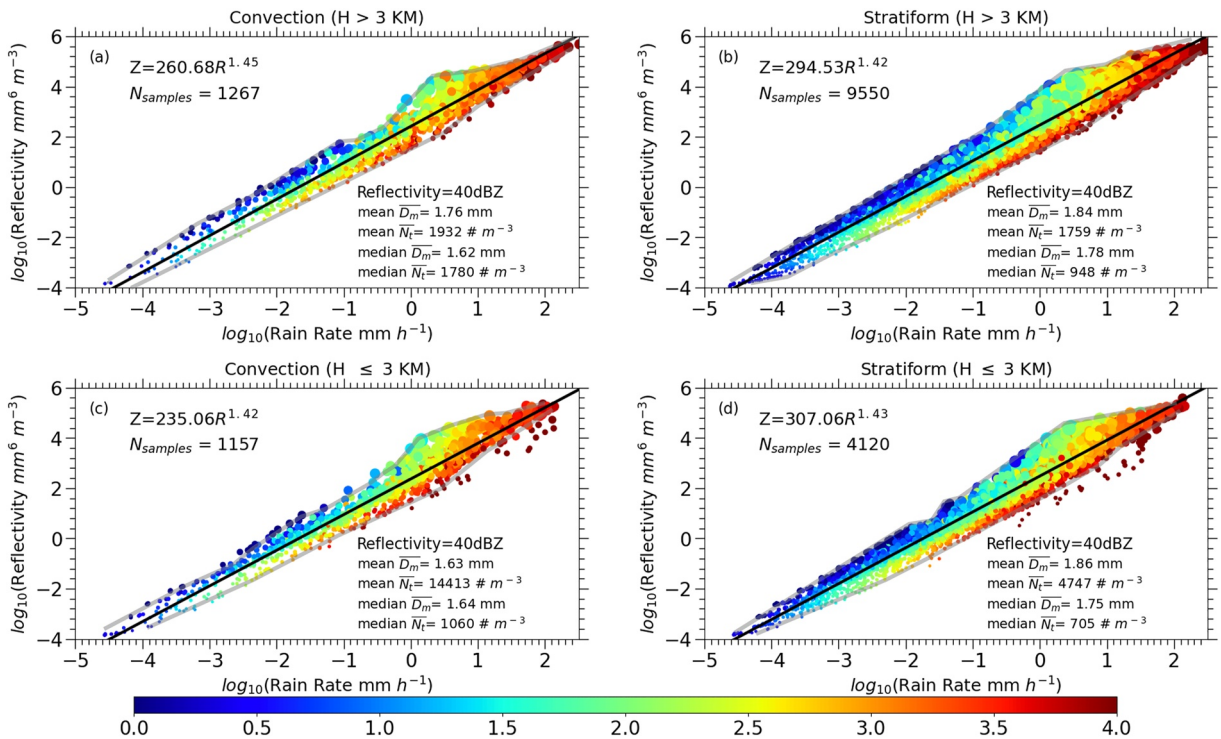

Figure 2. *Z-R* plots for (a) convective precipitation for samples collected at altitudes >3 km, and (b) stratiform precipitation for sample altitudes >3 km. (c and d) are the same as (a and b) but for samples altitudes ≤3 km. See text for the definition of convective and stratiform precipitation. The size of data points is proportional to D_m and the color is denoted by the N_t in the log scale. Line of best-fit derived from a linear least-squares method is drawn through the individual points and the corresponding equation is denoted in the top left of each plot. The number of samples ($N_{samples}$) is shown below the equation. The mean and median D_m and N_t for 40 dBZ are provided at the bottom right of each plot. The light gray lines above and below the best-fit line indicates the upper/left and lower/right boundary.

precipitation are based on Atlas et al. (2000), who used draft magnitude of $\approx 1\,m\,s^{-1}$ to separate convective precipitation and stratiform precipitation for data obtained in Tropical Ocean-Global Atmosphere Coupled Ocean-Atmosphere Response Experiment between 3.0 and 3.5 km altitude. There are two main differences between samples in our study and samples in Atlas et al. (2000). First, our samples are taken in hurricane environment. Second, the altitudes of our samples range from near surface to 7 km, although about half of the samples are taken near 3-km flight level. Given the wide range of altitudes where the samples are taken and strong vertical gradient of vertical motion, especially at low levels, in hurricane environment, we modified the $1\,m\,s^{-1}$ threshold value used in Atlas et al. (2000) to reflect that the magnitude of vertical motion tends to be weaker near surface and grows upward. Instead of using the same threshold for all altitudes, 0.3, 0.5, 0.7, 0.9, and 1 m s^{-1} are used for $H < 1$ km, 1 km $\leq H < 2$ km, 2 km $\leq H < 3$ km, 3 km $\leq H < 4$ km, and $H > 4$ km respectively because $|w|$ is small near the surface and at the low levels. The samples with $|w|$ less than the threshold value are flagged as stratiform precipitation. Otherwise, they are flagged as convective precipitation. All the integral variables in this plot, Z, R, D_m, and $N_{t,}$ are calculated directly from the observed RSDs. The most distinctive feature in all four groups is that the scatter of the Z-R distribution increases as reflectivity and rainfall rate increase up to 48 dBZ or 25 mm hr^{-1}, after which it decreases rapidly (slowly) along the upper/left boundary (lower/right boundary) of the scatter, converging rapidly (slowly) toward the fitted line. The scatter is indicative of the impact of RSDs on the Z-R relationships. As seen in Equation 1, Z is proportional to the number concentration and the sixth power of raindrop size. R (see Equation 2) is closely related to the number concentration and the third power of raindrop size. If the raindrop sizes are reduced by half, the number concentration needs to increase by a factor of 64 in order to achieve the same Z. The dramatic increase in the number concentration will lead to an increase in R by a factor of almost 8.

The widening of the spectrum in all four groups in Figure 2 indicates the growth phase of the precipitation, and shows the need for improving the rainfall estimations beyond a Z-R relationship with a constant coefficient and exponent. The fitted Z-R relationship can underestimate heavy rainfall by as much as 40% and overestimate light rainfall a few hundred percent when Z is between 30 and 50 dBZ. The narrowing of the spectrum when Z is >48 dBZ might reflect that RSDs are approaching equilibrium. Earlier studies (Hu & Srivastava, 1995; List et al., 1987; Srivastava, 1971; Willis, 1984) showed that RSDs reach equilibrium when raindrop coalescence and breakup are in balance, assuming no gain or loss of raindrops to other processes. The time required for reaching RSD equilibrium is shorter for greater R, because of the greater LWC and respectively shorter time between raindrop interactions. Rosenfeld and Ulbrich (2003) noted that the four Z-R relationships depicted by Atlas and Chmela (1957) when extended to large rainfall rates, tend to converge to the RSD equilibrium. After the RSDs reach equilibrium, the increase of R is due to the increase of number concentrations. Many other studies (e.g., Chang et al., 2009; Wen et al., 2018) also confirmed this early finding. The upper/left boundary (lower/right boundary) of the scatter converging rapidly (slowly) toward the fitted line in Figure 2 indicates that the breakup process dominates over the coalescence process during the evolution toward the equilibrium in this period and the mean drops sizes decrease slightly. Willis (1984) also showed the balance between coalescence and breakup appears to result in a larger relative decrease in the number concentrations at the large raindrop end of the spectrum than at the small to middle-sized ranges.

Although the general pattern of the Z-R distribution is very similar in all four groups, the coefficient and exponent in the Z-R relationship, D_m and N_t vary. The comparison between the Z-R relationships shown in Figures 2c and 2d, as well as with other Z-R relationships from previous studies is illustrated in Figure 3. In order to compare with other hurricane RSD studies, D_m and N_t for reflectivity 40 dBZ are provided. Note a range from 39.5 to 40.5 dBZ is used to represent 40 dBZ. Both mean and median D_m and N_t in each group are provided since sometimes the mean value can sometimes be misleading, especially for N_t if a few samples with extremely high values are included. Figure 2 shows that the convective regions for both $H \leq 3$ km and $H > 3$ km have relatively smaller drops, but much higher number concentration compared to the stratiform regions. This is consistent with earlier studies (e.g., Rosenfeld & Ulbrich, 2003). Tokay et al. (2008) showed that the number concentration was 700 ± 100 drops m^{-3} and D_m was 1.67 ± 0.3 mm, using JW disdrometer data from 7 tropical cyclones in the Atlantic basin. Both the mean and median D_m from our study is very close to that from Tokay et al. (2008, thereafter T2008). On the other hand, N_t is significantly higher than that in T2008, especially for the convective precipitation. This discrepancy might arise because the JW disdrometer underestimates the small raindrops (T2008), which both Z and D_m are not sensitive to.

(a)

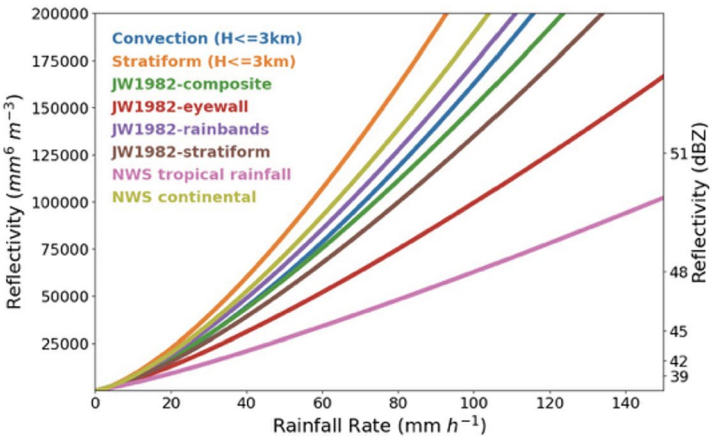

(b) Computed rainfall (mm h-1) as a function of reflectivity (dBZ)

Z-R equation		Reflectivity (dBZ)				
Source	Equation	30	35	40	45	50
C (H ≤ 3 km)	$Z=235R^{1.42}$	2.8	6.2	14.0	31.6	71.0
S (H ≤ 3 km)	$Z=307R^{1.43}$	2.3	5.1	11.4	25.6	57.2
JW1982-composite	$Z=300R^{1.35}$	2.4	5.7	13.4	31.5	73.9
JW1982-eyewall	$Z=287R^{1.27}$	2.7	6.6	16.4	40.5	100.4
JW1982-rainband	$Z=301R^{1.38}$	2.4	5.5	12.7	29.2	67.2
JW1982-stratiform	$Z=269R^{1.35}$	2.6	6.2	14.6	34.2	80.1
NWS TR	$Z=250R^{1.2}$	3.2	8.3	21.6	56.5	147.4
NWS CC	$Z=300R^{1.4}$	2.4	5.4	12.2	27.9	63.4

Figure 3. (a) *Z-R* relationships for convection precipitation and stratiform precipitation for $H \leq 3$ km from this study, JW1982-composite, JW1982-eyewall, JW1982-rainbands, JW1982-stratiform, NWS tropical rainfall and NWS continental rainfall. (b) The corresponding *Z-R* equations and computed rainfall (values within cells in mm h^{-1}) as a function of reflectivity for the *Z-R* relationships shown in (a).

4. Compare *Z-R* Relationships With Previous Studies

We next compare *Z-R* relationships from this study to selected *Z-R* relationships from the literature. Since our data source is closest to JW1982, four *Z-R* relationships from JW1982 are selected for comparison. *Z-R* relationships adopted by National Weather Service (NWS) for continental and tropical rainfall (Fulton et al., 1998) are also selected. Since all the data from JW1982 are sampled at or lower than 3-km altitude and NWS *Z-R* relationships are from a surface disdrometer, only *Z-R* relationships for convective and stratiform precipitation at $H \leq 3$ km from Figure 2 are used here.

Figure 3 shows that the stratiform relationship from this study (orange line) is the leftmost curve, which implies that it has the largest raindrop sizes and the smallest number concentrations for a given Z among all the *Z-R* relationships shown here. In contrast, the convective relationship (blue line) has relatively higher concentration and smaller raindrop sizes compared to the stratiform relationship, consistent with Figure 2 and previous studies (e.g., Rosenfeld & Ulbrich, 2003). Comparing the *Z-R* for the convective precipitation from this study and the JW1982-composite reveals that these two *Z-R* relationships generate similar rainfall rate for $Z < 48$ dBZ. JW1982 produces slightly higher rainfall for $Z > 48$ dBZ. Since the majority of samples from the JW1982 composite are convective, this result seems to imply the *Z-R* relationship for the convective precipitation in hurricanes is relatively robust. However, if this *Z-R* relationship applies to the entire hurricane, it will tend to overestimate the rainfall. As shown in Figure 2, the majority of the samples are from stratiform precipitation and the areal coverage of stratiform precipitation in hurricanes is much larger than the convective coverage. As noted in Marks and Houze (1987, thereafter MH1987), more than half of the rainfall in the inner core of Hurricane Alicia is from stratiform precipitation.

The comparison of JW1982-eyewall and JW1982-rainband reveals that the eyewall (rainband) is associated with smaller (larger) drops and larger (smaller) number concentration and consequently the estimated rainfall is higher for the eyewall for a given Z. When Z reaches 50 dBZ, the difference can be as much as 33 mm hr^{-1}. Therefore, the heavy rainfall in hurricanes tends to occur in the eyewall (e.g., MH1987; JW1982; Black & Hallett, 2012). Earlier studies (e.g., Atlas et al., 1963; MH1987) characterized the eyewall as having large radial and small vertical gradients of reflectivity associated with convective precipitation and the rainbands as having large vertical and small radial gradient of reflectivity associated with stratiform precipitation. If this statement holds for JW1982, then their results also indicate the smaller drops and larger number concentrations for convective precipitation. Yet JW1982 noted that their rainband samples are composed of both stratiform and convective rain in approximately a 1:1 ratio and provided a separate *Z-R* relationship for the stratiform in the rainband, which is shown by the brown line in Figure 3.

The comparison of the *Z-R* relationship for the stratiform portion in the rainband and that for the entire rainband sample implies that the convective portion of the rainband is composed of even larger drops than that in the stratiform portion. One possible explanation for this discrepancy is that the cold rain process might play an important role in the convective precipitation of the rainbands in JW1982. Hu et al. (2020) analyzed the WSR-88D dual-polarization radar data for Hurricane Harvey in 2017 and showed that the retrieved D_m for the ice particles associated with the convection in the rainbands is much larger than that in the eyewall. This indicates the presence of graupel, which will melt into raindrops when passing through the melting level and continue to grow through coalescence into bigger raindrops.

Marks (1985) and Hu et al. (2020) also showed that the bright band is more pronounced in the eyewall than in the rainbands and the echo top is higher in the rainbands. While this would appear to contradict the early view of hurricane eyewall and rainbands, the structure of the eyewalls and rainbands is ever-changing and what is captured by the observation depends on the stage of the eyewall and rainbands and where the observations are taken. As noted by MH1987 in their study of Hurricane Alicia, although most of the data showed distinct differences between the eyewall and rainbands, one exception appeared at landfall when vertical structure of the eyewall echoes was similar to those outside the eyewall.

The *Z-R* relationships for tropical rainfall and continental rainfall employed by NWS (Fulton et al., 1998) are also shown in Figure 3. The rainfall calculated from the *Z-R* relationship for tropical rainfall will significantly overestimate the rainfall in hurricanes, especially in the rainbands and stratiform region. Figure 2 shows large scatter in *Z-R* distribution and the scatter is closely related to drop sizes. Figure 3 indicates that the composite *Z-R* relationships for hurricanes do not change significantly. However, the large differences in the *Z-R* relationships from different regions of hurricanes suggest that in order to accurately estimate rainfall for a specific time at a specific location, the *Z-R* relationship needs to be improved beyond a power-law with constant coefficient and exponent. The scatter of *Z-R* relationship is closely related to D_m, which is proportional to differential radar reflectivity Z_{dr} (Bringi et al., 2003) that can be measured by dual-polarized radar. This suggests that the *Z-R* relationship can be improved by including the information of D_m.

5. Improve *Z-R* Relationship Using Random Reforest Regression Model

The application of machine learning and artificial intelligence in meteorology has grown rapidly in last decade (e.g., Gagne et al., 2017; McGovern et al., 2019). RandomForests (hereafter RFs) (Breiman, 2001) is a simple and powerful algorithm with a strong track record (Gagne et al., 2014; Herman & Schumacher, 2018). RFs learn an ensemble of decision trees, each of which is trained on a separate bootstrap resampled data set and using a different subset of the attributes. In this study, we use two attributes, radar reflectivity and mass-weighted-diameter, for the RFs input. The rainfall rate calculated from the observed RSDs is used as the output for the RFs. 70% of the entire 18,076 samples are used for the training data and 30% for the test data. Twenty trees are used for the RFs. Sensitivity tests show that using more trees (up to 100) does not degrade the performance of the trained model but slows down the training process. The input that only includes two attributes might not fully tap the potential of the RFs but the performance of RFs is significantly better than a single decision tree regression model. Other machine learning models, such as support vector regression and k-nearest neighbors regression are also tested but the RFs outperform both of them, although only marginally.

Figure 4a shows the scatter plot of observed rainfall rate (abscissa) in the test data versus the rainfall rate estimated (ordinate) from the *Z-R* relationship, which is developed from the training data set (i.e., 70% of the entire 18,076 samples as used in RFs) through least square fitting. As we can see, such *Z-R* relationship overestimates the low and middle rainfall rate ($\leq$40 mm hr^{-1}) and underestimates the high rainfall rate (>40 mm hr^{-1}) for most of the samples in the test data. Figure 4b is similar to Figure 4a but the ordinate is rainfall rate predicted by the RFs. Figure 4b clearly demonstrates that including mass-weighted-diameter reduces uncertainties in the estimated rainfall. R^2 improves from 0.8 in Figures 4a to 0.9 in Figure 4b. Both the overestimation for the low and middle rainfall rate and underestimation for the high rainfall rate are alleviated. Yet the error for the high rainfall rate remains large. This issue arises due to the insufficient number of samples with high rainfall rate.

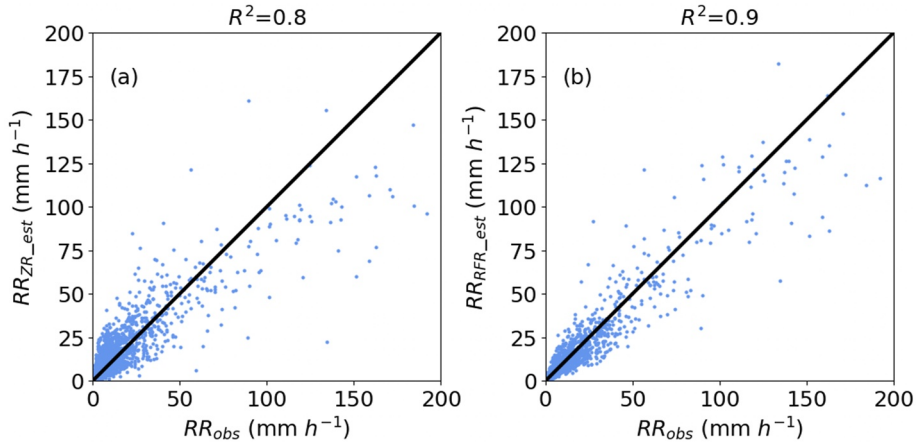

Figure 4. scatter plots of (a) rainfall rate calculated from the observed Raindrop Size Distribution (RSD) versus rainfall rate estimated from the composite *Z-R* relationship, (b) rainfall rate calculated from the observed RSD versus rainfall rate estimated from combining the composite *Z-R* relationship and the random forest regression model for test data (see text for details). Black line in each plot indicates the perfect estimation (estimation = observation).

6. Conclusions and Discussion

RSDs collected by PIP from 17 flights through 6 hurricanes during hurricane field program in 2020 are used to study *Z-R* relationship. The results show that the *Z-R* relationship is highly scattered. The scatter increases with rainfall and reflectivity up to 48 dBZ or 25 mm hr^{-1}, after which it decreases rapidly. The difference in the rainfall rate when reflectivity is 40 dBZ can be as large as 50 mm hr^{-1}. Although a *Z-R* relationship from a composite might give a reasonable estimate for the overall accumulated rainfall, the rainfall estimate at a specific time and specific location can deviate significantly from what the composite *Z-R* relationship gives due to the scatter. The usage of RFs demonstrates that including the mass-weighted-diameter along with radar reflectivity improves the rainfall estimation significantly, especially for low and middle rainfall rate where majority of the samples are. Increasing the samples in high rainfall rate is expected to improve the rainfall estimation for high rainfall rate as machine learning models can only forecast the scenarios they have seen.

One caveat on the effort of estimating rainfall rate from radar reflectivity and mass-weighted-diameter is that there are innate uncertainties, which will not be eliminated even with the most sophisticated machine learning models and a large volume of samples. Using radar reflectivity and mass-weighted-diameter to estimate rainfall rate can be interpreted as using two moments of the RSDs to forecast another moment. Most of RSDs can be approximated as three-parameter gamma distributions, as shown in the literature (e.g., Ulbrich & Atlas, 1998). Three moments are required to fully determine the gamma distribution. When there are only two moments available, such as radar reflectivity and mass-weighted-mean-diameter, there are uncertainties in the gamma distribution as well as in any other moments calculated from the gamma distribution.

Data Availability Statement

The authors express thanks to NOAA/HRD Data Support for providing the microphysics observation data (https://www.aoml.noaa.gov/hrd/data_sub/hurr2020.html).

Acknowledgments
This research was supported by the Office of Atmospheric Research/Weather Portfolio, the Atlantic Oceanic and Meteorological Laboratory, and the National Weather Service/Office of Science Technology Integration, United Forecast Research to Operation project of the National Oceanographic and Atmospheric Administration. The authors want to acknowledge our colleagues: Drs. Paul Reasor and John Gamache, for their insightful comments to improve this manuscript during our internal review.

References

Atlas, D., & Chmela, A. C. (1957). Physical-synoptic variations of drop-size parameters. In *Proceedings of sixth weather radar conference. program* (Vol. 4, pp. 21–29). American Meteorological Society.

Atlas, D., Hardy, K., Wexler, R., & Boucher, R. (1963). The origin of hurricane spiral bands. *Geofísica Internacional*, *3*, 123–132.

Atlas, D., Ulbrich, C. W., Marks, F. D., Jr., Black, R. A., Amitai, E., Willis, P. T., & Samsury, C. E. (2000). Partitioning tropical oceanic convective and stratiform rains by draft strength. *Journal of Geophysical Research*, *105*(D2), 2259–2267. https://doi.org/10.1029/1999jd901009

Battan, L. J. (1973). *Radar observation of the atmosphere*. The University of Chicago Press.

Black, R. A., & Hallett, J. (2012). Rain rate and water content in hurricanes compared with summer rain in Miami, Florida. *Journal of Applied Meteorology*, *51*(12), 2218–2235. https://doi.org/10.1175/jamc-d-11-0144.1

Breiman, L. (2001). Random forests. *Machine Learning*, *45*(1), 5–32.
Bringi, V. N., Chandrasekar, V., Hubbert, J., Gorgucci, E., Randeu, W. L., & Schoenhuber, M. (2003). Raindrop size distribution in different climatic regimes from disdrometer and dual-polarized radar analysis. *Journal of the Atmospheric Sciences*, *60*(2), 354–365. https://doi.org/10.1175/1520-0469(2003)060<0354:rsdidc>2.0.co;2
Chang, W.-Y., Wang, T.-C. C., & Lin, P.-L. (2009). Characteristics of the raindrop size distribution and drop shape relation in typhoon systems in the Western Pacific from the 2D video disdrometer and NCU C-band polarimetric radar. *Journal of Atmospheric and Oceanic Technology*, *2610*(10), 1973–1993. https://doi.org/10.1175/2009jtecha1236.1
Donnadieu, G. (1982). Observation de deux changements das spectres des gouttes de pluie dans une averse de nuages stratiformes. *Journal de Recherches Atmospheriques*, *14*, 439–455.
Fulton, R. A., Breidenbach, J. P., Seo, D.-J., Miller, D. A., & O'Bannon, T. (1998). The WSR-88D rainfall algorithm. *Weather and Forecasting*, *13*(2), 377–395. https://doi.org/10.1175/1520-0434(1998)013<0377:twra>2.0.co;2
Gagne, D. J., McGovern, A., Haupt, S. E., Sobash, R. A., Williams, J. K., & Xue, M. (2017). Storm-based probabilistic hail forecasting with machine learning applied to convection-allowing ensembles. *Weather and Forecasting*, *32*, 1819–1840. https://doi.org/10.1175/WAF-D-17-0010.1
Gagne, D. J., McGovern, A., II, & Xue, M. (2014). Machine learning enhancement of storm-scale ensemble probabilistic quantitative precipitation forecasts. *Weather and Forecasting*, *29*(4), 1024–1043. https://doi.org/10.1175/waf-d-13-00108.1
Herman, G. R., & Schumacher, R. S. (2018). Money doesn't grow on trees, but forecasts do: Forecasting extreme precipitation with random forests. *Monthly Weather Review*, *146*(5), 1571–1600. https://doi.org/10.1175/mwr-d-17-0250.1
Hu, J., Rosenfeld, D., Ryzhkov, A., & Zhang, P. (2020). Synergetic use of the WSR-88D radars, GOES-R satellites, and lightning networks to study microphysical characteristics of hurricanes. *Journal of Climate and Applied Meteorology*, *59*(6), 1051–1068. https://doi.org/10.1175/jamc-d-19-0122.1
Hu, Z., & Srivastava, R. (1995). Evolution of the raindrop size distribution by coalescence, breakup and evaporation: Theory and observations. *Journal of the Atmospheric Sciences*, *52*(10), 1761–1783. https://doi.org/10.1175/1520-0469(1995)052<1761:eorsdb>2.0.co;2
Jorgensen, D. P., & Willis, P. T. (1982). A Z–R relationship for hurricanes. *Journal of Applied Meteorology*, *21*(3), 356–366. https://doi.org/10.1175/1520-0450(1982)021<0356:azrrfh>2.0.co;2
List, R., Low, T. B., Donaldson, N., Freire, E., & Gillespie, J. R. (1987). Temporal evolution of drop spectra to collisional equilibrium in steady and pulsating rain. *Journal of the Atmospheric Sciences*, *44*(2), 362–372. https://doi.org/10.1175/1520-0469(1987)044<0362:teodst>2.0.co;2
Marks, F. D. (1985). Evolution of the structure of precipitation in hurricane Allen (1980). *Monthly Weather Review*, *113*(6), 909–930. https://doi.org/10.1175/1520-0493(1985)113<0909:eotsop>2.0.co;2
Marks, F. D., & Houze, R. A. (1987). Inner core structure of Hurricane Alicia from airborne Doppler radar observations. *Journal of the Atmospheric Sciences*, *44*(9), 1296–1317. https://doi.org/10.1175/1520-0469(1987)044<1296:icsoha>2.0.co;2
Marshall, J. S., & Palmer, W. H. (1948). The distribution of raindrops with size. *Journal of Meteorology*, *5*(4), 165–166. https://doi.org/10.1175/1520-0469(1948)005<0165:tdorws>2.0.co;2
McGovern, A., Gagne, D. J., II, Lagerquist, R., Elmore, K., Jergensen, G. E., Homeyer, C. R., & Smith, T. (2019). Making the black box more transparent: Understanding the physical implications of machine learning. *Bulletin of the American Meteorological Society*, *100*(11), 2175–2199. https://doi.org/10.1175/bams-d-18-0195.1
Rosenfeld, D., & Ulbrich, C. W. (2003). Cloud microphysical properties, processes, and rainfall estimation opportunities. In *Radar and atmospheric science: A collection of essays in honor of david Atlas, meteor. Monogr, No. 52* (pp. 237–258). American Meteorological Society.
Srivastava, R. C. (1971). Size distribution of raindrops generated by their breakup and coalescence. *Journal of the Atmospheric Sciences*, *28*(3), 410–415. https://doi.org/10.1175/1520-0469(1971)028<0410:sdorgb>2.0.co;2
Steiner, M., Smith, J. A., & Uijlenhoet, R. (2004). A microphysical interpretation of radar reflectivity–rain rate relationships. *Journal of the Atmospheric Sciences*, *61*(10), 1114–1131. https://doi.org/10.1175/1520-0469(2004)061<1114:amiorr>2.0.co;2
Tokay, A., Bashor, P. G., Habib, E., & Kasparis, T. (2008). Raindrop size distribution measurements in tropical cyclones. *Monthly Weather Review*, *136*(5), 1669–1685. https://doi.org/10.1175/2007mwr2122.1
Ulbrich, C. W. (1983). Natural variations in the analytical form of the raindrop size distribution. *Journal of Climate and Applied Meteorology*, *22*(10), 1764–1775. https://doi.org/10.1175/1520-0450(1983)022<1764:nvitaf>2.0.co;2
Ulbrich, C. W., & Atlas, D. (1998). Rainfall microphysics and radar properties: Analysis methods for drop size spectra. *Journal of Applied Meteorology*, *37*(9), 912–923. https://doi.org/10.1175/1520-0450(1998)037<0912:rmarpa>2.0.co;2
Ulbrich, C. W., & Lee, L. G. (2002). Rainfall characteristics associated with the remnants of tropical storm Helene in upstate South Carolina. *Weather and Forecasting*, *17*(6), 1257–1267.
Waldvogel, A. (1974). The N0 jump of raindrop spectra. *Journal of the Atmospheric Sciences*, *31*(4), 1067–1078. https://doi.org/10.1175/1520-0469(1974)031<1067:tjors>2.0.co;2
Wen, L., Zhao, K., Chen, G., Wang, M., Zhou, B., Huang, H., et al. (2018). Drop size distribution characteristics of seven typhoons in China. *Journal of Geophysical Research: Atmospheres*, *123*, 6529–6548. https://doi.org/10.1029/2017JD027950
Willis, P. T. (1984). Functional fits to some observed drop size distributions and parameterization of rain. *Journal of the Atmospheric Sciences*, *41*(9), 1648–1661. https://doi.org/10.1175/1520-0469(1984)041<1648:fftsod>2.0.co;2

References From the Supporting Information

Black, R. A., & Hallett, J. (1986). Observations of the distribution of ice in hurricanes. *Journal of the Atmospheric Sciences*, *43*(8), 802–822. https://doi.org/10.1175/1520-0469(1986)043<0802:ootdoi>2.0.co;2
Korolev, A. (2007). Reconstruction of the sizes of spherical particles from their shadow images. Part I: Theoretical considerations. *Journal of Atmospheric and Oceanic Technology*, *24*(3), 376–389. https://doi.org/10.1175/jtech1980.1